An Electrothermally Actuated VO_2-Based MEMS Using Self-Sensing Feedback Control

Emmanuelle Merced, *Student Member, IEEE*, David Torres, Xiaobo Tan, *Senior Member, IEEE*, and Nelson Sepúlveda, *Senior Member, IEEE*

***Abstract*— A self-sensing approach is used to accurately control the large displacements observed in VO_2-based microelectromechanical systems actuators. The device is operated electrothermally using integrated resistive heaters. The coupling of the abrupt electrical and mechanical changes in VO_2 films across its phase transition allow for the estimation of the device's deflection by monitoring the film's resistance. Furthermore, the typical hysteretic behavior observed in VO_2 films is significantly reduced in the present device and the need for optical testing equipment is eliminated. The displacement-resistance relationship is modeled by a memoryless Boltzmann function consisting of four parameters, which are optimized to fit the experimental data with an average error of 1.1 μm throughout the complete actuation range of 95 μm. The estimated deflection is used as feedback to achieve closed-loop micropositioning control of the device, which is designed from the system dynamics obtained experimentally. Closed-loop sinusoidal and step reference response experiments are performed in order to show the effectiveness of the self-sensing feedback technique used. In the closed-loop sinusoidal frequency response, a cutoff frequency of 43 Hz is observed with a maximum actual deflection error of 0.19 dB up to the phase margin frequency of 30 Hz. In the step response, an average actual displacement steady-state error of ±1.15 μm is obtained with response times ranging from 5 to 12 ms. [2014-0038]**

***Index Terms*— Vanadium dioxide, MEMS actuator, self-sensing feedback, phase transition.**

I. Introduction

ACCURATE displacement control in MEMS-based actuators has been a subject of research for use as an integral part in a variety of applications, such as positioners [1]–[3], grippers [4], [5], motors [6], [7], valves [8], and biomedical equipment [9]–[11]. Although the techniques used to control MEMS actuators vary depending on the actuation mechanism used, the end goal of every approach is to minimize the difference between the desired and actual output through some control effort. Some of the controllers used for micro-actuation are linear compensators (e.g., proportional-integral-derivative (PID) and linear quadratic regulators (LQR)) [12], [13], nonlinear compensators (e.g., sliding mode control) [14], and fuzzy controllers [15]. The performance of these controllers greatly depends on the accuracy and effectiveness of the sensing mechanism used to measure the output.

Different approaches have been developed to accurately measure or estimate the displacements of MEMS-based actuators and implement the controllers mentioned above. These techniques can be divided into two main groups: 1) internal sensors, such as capacitive plates [16], piezoresistors [17], and resistance strain gauges [18]; and 2) external sensors, such as light scattering techniques [19], and interferometry [20]. Internal sensors complicate the fabrication of the MEMS devices; and those based on capacitive sensing are limited to smaller displacements. On the other hand, external sensors require the use of bulky and high cost measurement setups. Self-sensing is yet another technique for measuring displacements, in which the deflection is estimated based on some other material parameter change, such as resistance or permittivity [21]–[23]. This method is particularly popular in smart material-based MEMS actuators, such as shape memory alloys (SMAs), piezoelectrics, and electroactive polymers, where usually more than one material parameter is sensitive to the actuation signal. In addition, since the smart material itself serves as the sensor, no additional sensing elements are needed. However, the inherent hysteresis behavior observed in many smart materials greatly complicates their use, which in addition requires methods for hysteresis cancellation, such as hysteresis compensation through modeling [24], [25], external manipulation [26], or by limiting the actuation range of the device [27]. More recently, a naturally occurring hysteresis cancellation effect based on self-sensing has been observed in vanadium dioxide (VO_2)-based MEMS devices, where the relationship between device deflection and VO_2 resistance shows a dramatic reduction in the hysteresis due to the strong correlation between the parameters [28].

VO_2 is a stable vanadium oxide phase known to undergo abrupt changes in its electrical [29], mechanical [19], and optical [30] properties during its solid-to-solid phase transition, which can be induced thermally at a temperature of approximately 68 °C. A strain energy density of $8.1 \times 10^5\,\mathrm{J\,m^{-3}}$ and curvature changes greater than $2000\,\mathrm{m^{-1}}$ have been obtained in VO_2-coated silicon (Si) structures [31]. This behavior is a consequence of the abrupt change in crystallographic structure of the VO_2, during which the plane parallel to the substrate contracts abruptly from the $(011)_M$ to the

Manuscript received February 4, 2014; revised April 9, 2014; accepted April 10, 2014. Date of publication May 7, 2014; date of current version January 30, 2015. This work was supported by the National Science Foundation under Grant ECCS 1306311 and Grant CMMI 1301243. The work of E. Merced was supported by the National Science Foundation under Grant DGE-0802267 through the Graduate Research Fellowship Program. Subject Editor S. M. Spearing.

The authors are with the Department of Electrical and Computer Engineering, Michigan State University, East Lansing, MI 48824 USA (e-mail: mercedem@egr.msu.edu; torresd5@egr.msu.edu; xbtan@egr.msu.edu; nelsons@egr.msu.edu).

Color versions of one or more of the figures in this paper are available online at http://ieeexplore.ieee.org.

Digital Object Identifier 10.1109/JMEMS.2014.2317944

$(110)_R$ — where M and R stand for monoclinic and rutile phases, respectively — causing large strain changes. The transition is fully reversible and has been successfully integrated into electro-thermally driven MEMS-based silicon dioxide (SiO_2) cantilevers in order to achieve out-of-plane tip displacements comparable to the cantilever length through a small current operating window [32], [33]. Another work done by the authors explored the self-sensing feedback control of a micro-actuator using VO_2 resistance measurements from a film deposited on a separate substrate [28]. Since both parameters were measured in separate locations, a hysteresis still remained present between them. In addition, the actuation was induced by a Peltier heater to which the sample was attached, making the system slow and bulky.

The work presented here shows a highly accurate closed-loop controlled MEMS-based actuator with an integrated heater and sensor, which uses a self-sensing approach that drastically reduces the measurement hysteresis throughout the complete actuation range. Self-sensing is achieved by estimating the actual deflection through a resistance-to-deflection Boltzmann model obtained after a parameter fitting using simultaneous *in situ* VO_2 resistance and deflection measurements. The estimated deflection is then used in feedback with a proportional-integral (PI) controller in order to accurately control the MEMS actuator. The improvements over previous published work done by the authors are: 1) device miniaturization through the successful fabrication of a MEMS actuator with monolithically integrated heater and sensor (using self-sensing), 2) the capability of simultaneous *in situ* VO_2 resistance and actuator deflection measurements, and 3) a deflection and resistance dynamic model for design of closed-loop controlled actuator that achieves higher actuation bandwidths and lower error (both transient and steady-state).

The rest of this document is organized as follows. A detailed device fabrication and measurement setup used for model determination and self-sensing control implementation is presented in Section II. Section III shows the quasi-static results used to obtain the self-sensing model, the resistance and deflection frequency responses used to obtain the actuator dynamic model, and the PI controller design. Section IV contains the results and discussions of the implemented self-sensing feedback system, which includes the closed-loop frequency response of the MEMS actuator, and step and sinusoidal reference responses. Lastly, Section V includes some concluding remarks and future work.

II. Experimental Procedures

A. Device Fabrication and VO_2 Deposition

The VO_2-based MEMS actuator used in this work consisted of a titanium/platinum (Ti/Pt) electrode sandwiched between two layers of SiO_2 with a VO_2 layer on top of the device. Since both SiO_2 layers have very similar thicknesses, the thermal stress of this SiO_2-Ti/Pt-SiO_2 structure is nearly canceled. A rendering of the fabrication process flow steps is shown in Figure 1 along with a description of each step. A 1 µm layer of SiO_2 was deposited on the polished side of a (100) Si wafer using low thermal oxide (LTO). After the SiO_2 deposition,

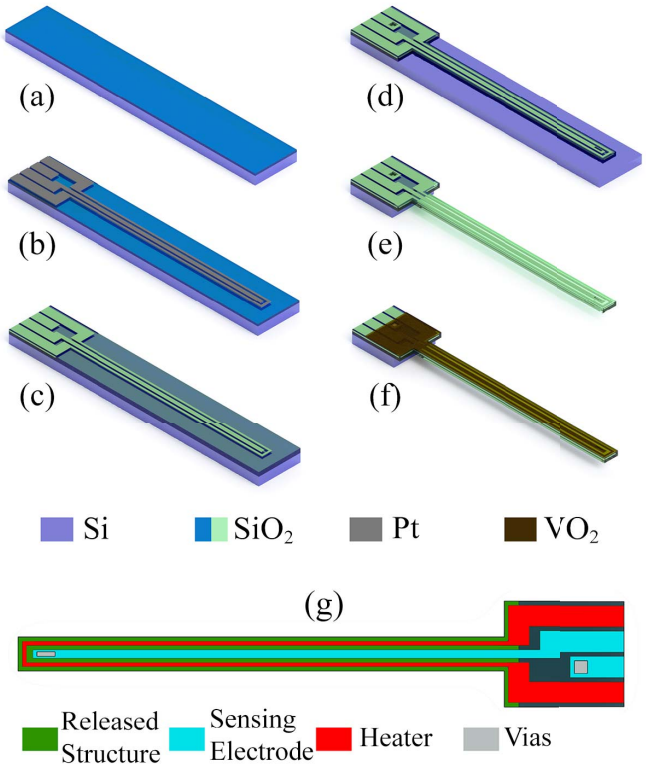

Fig. 1. Fabrication process flow of the VO_2-MEMS-actuator. (a) Deposition of SiO_2 by LTO (first layer), (b) thermal evaporation of Pt and pattern by lift-off, (c) deposition of SiO_2 by LTO (second layer), (d) DRIE etching of SiO_2 for device pattern, (e) MEMS release by XeF_2 etching of Si, (f) Deposition of VO_2 by PLD, (g) Top view of the device.

the wafer was cleaned and prepared for lift-off using a two layer resist of lift-off resist (LOR A) and standard positive photoresist (Shipley 1813). A combination layer of Ti/Pt (500 Å/1500 Å) was deposited through thermal evaporation followed by a lift-off step using solvent (Remover PG) and then cleaned using photoresist removal (NanoStrip). The Ti layer is used for adhesion between the Pt and the SiO_2 layers. A second 1 µm SiO_2 layer was deposited on top of the patterned Pt using LTO. This oxide layer serves to electrically isolate the Pt and the VO_2 deposited in the final step. The wafer was then patterned (using Shipley 1813) to define the micro-actuator structure to be released, the wire bonding pads, and the vias that will expose the Pt to the VO_2 in the cantilever (see Figure 2-a). Deep reative ion etching (DRIE) was used to etch the SiO_2 on the exposed areas until the Pt and Si were revealed. The wafer was partially diced into 0.25×0.25 inch dies and the MEMS actuators were then released using xenon difluoride (XeF_2). After performing the release step, a 200 nm VO_2 layer was deposited using pulsed laser deposition (PLD).

During the PLD deposition process, an individual die was placed on a rotating holder in order to ensure uniform thickness and temperature distribution through the deposition process. A shadow mask was placed directly on top of the die to protect the wire bonding pads from the VO_2 deposition. Before deposition, a background pressure of 5×10^{-6} Torr was reached. Then, a heater located at the back of the sample was controlled to a temperature of 550 °C under an oxygen atmosphere with pressure of 15 mTorr. A krypton

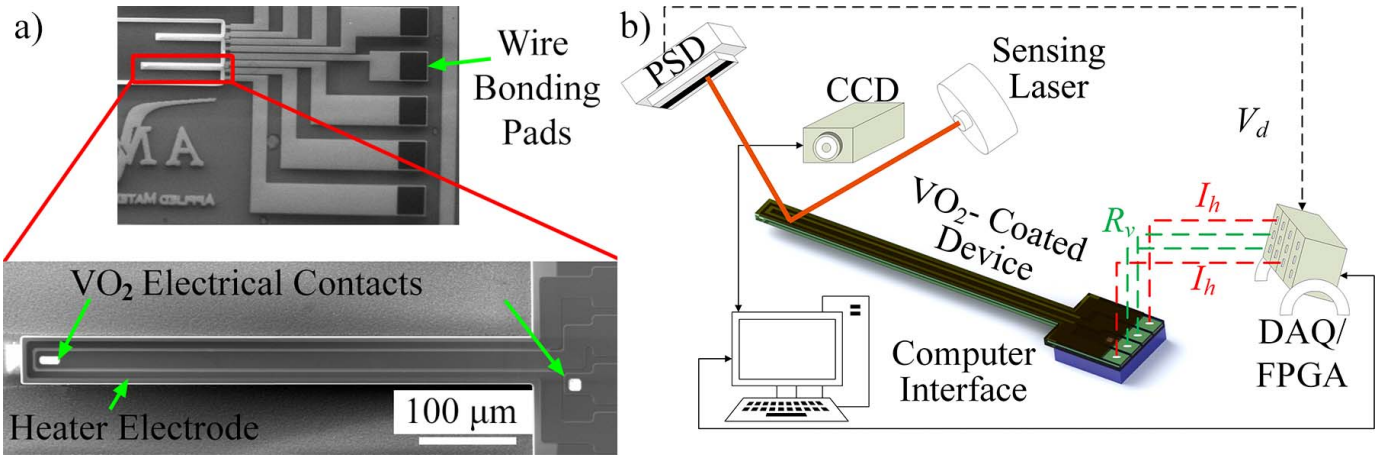

Fig. 2. (a) SEM images of the finalized device. The two small rectangles near the anchor and near the tip are the vias between the Pt and the VO_2 and the heater is complete isolated from the VO_2. More detailed SEM images of this device can be found in [34]. (b) Measurement setup for performing the characterization and control experiments on the actuator. The setup is capable of *in situ* resistance and deflection measurements.

fluoride (KrF) excimer laser with energy of 350×10^{-3} J and a repetition rate of 10 Hz was then focused on a rotating metallic vanadium target. The deposition time was 30min and it was followed by another 30min of annealing under same conditions. The finalized device consists of a 550 µm long and 50 µm wide micro-cantilever with Pt trace dimensions of 8 µm for the heater and 18 µm for the VO_2 resistance measurement electrodes (see Figure 2-a). After deposition the die was placed on a integrated circuit (IC) package and wire bonded to create the electrical contacts to the Pt heater and the VO_2.

B. Electro-Mechanical Measurement Setup

The IC package containing the VO_2-MEMS actuator was placed on the measurement setup shown in Figure 2-b in order to perform the simultaneous *in situ* VO_2 resistance and deflection measurements used in the characterization and control of the device using self-sensing. For deflection measurements, a sensing laser ($\lambda = 808$ nm) was focused at the tip of the cantilever and the reflected light was aimed at a position sensitive detector (PSD). The output of the PSD is a voltage (V_d) proportional to the position of the incident light in the active area. Using side view images from a charge-couple device (CCD) camera at different actuation values, V_d was calibrated to actual deflection (D_r). For VO_2 resistance measurements, a constant current of 15 µA was applied to the VO_2 through the inner Pt electrode along the actuator ("VO_2 Electrical Contacts" labeled on Figure 2-a and green dashed lines in Figure 2-b) while the voltage was being measured. It was verified that this current value did not cause actuator deflection; i.e. self-heating due to this current only was not large enough to cause actuation. Using Ohm's Law, the VO_2 resistance (R_v) is then calculated. A data acquisition system and field programmable gate array (DAQ/FPGA) supplies the actuation signal (I_h) to the Pt heater ("Heater Electrode" labeled on Figure 2-a and red dashed lines in Figure 2-b) and measures the corresponding voltage input signals (from the PSD and the "VO_2 Electrical Contacts"), which are then used to calculate R_v and D_r. The DAQ/FPGA can be configured to operate either in open- or closed-loop using a computer interface.

III. Theory

A. Self-Sensing Model

The measurement setup was used to obtain quasi-static simultaneous R_v and D_r curves as a function of I_h, which are shown in Figure 3-(a-b). For this experiment, a series of decreasing first order reversal curves were obtained in order to cover the hysteresis minor loops. The current range for the complete experiment is from 1.8 to 5.2 mA in steps of 30 µA. In order to measure steady-state values for R_v and D_r a wait time of 4 s was selected between each current setpoint. The VO_2 resistance shows the typical nonlinear hysteretic behavior observed in similar deposited films on SiO_2 with a maximum resistance change of $8 \times 10^5\ \Omega$ [33]. The deflection range obtained for the actuation region (which spans less than 1 mA change in I_h, -see Figure 3-b) was 95 µm. Note that the operational region is defined as the region through which monotonic deflection across the VO_2 transition occurs in the actuator. There are two competing mechanisms that affect the deflection of the device: the structural phase transition of the VO_2 layer and the differential thermal expansion. The former is responsible for the large positive change in deflection across the phase transition, while the latter is responsible for the small negative changes at both ends. This non-monotonic behavior has been observed in the past and a detailed discussion is given in [19] and [31].

Figure 3-(c) shows the relationship between deflection and VO_2 resistance for the same experimental data. The hysteresis is greatly reduced due to the highly coupled mechanisms responsible for the electrical — product of the insulator-to-metal transition (IMT) — and mechanical changes — product of the structural phase transition (SPT) — in the VO_2. A Boltzmann function is then used to model the self-sensing relationship. The Boltzmann function is defined by

$$\hat{D}_r = \frac{A_1 - A_2}{1 + \exp\left(R_v - x_0\right)/dx} + A_2, \tag{1}$$

where A_1, A_2, x_0 and dx are the model parameters, which are obtained through a nonlinear model fit using a conjugated gradient method, and $\hat{D}_r$ is the estimated deflection. The model

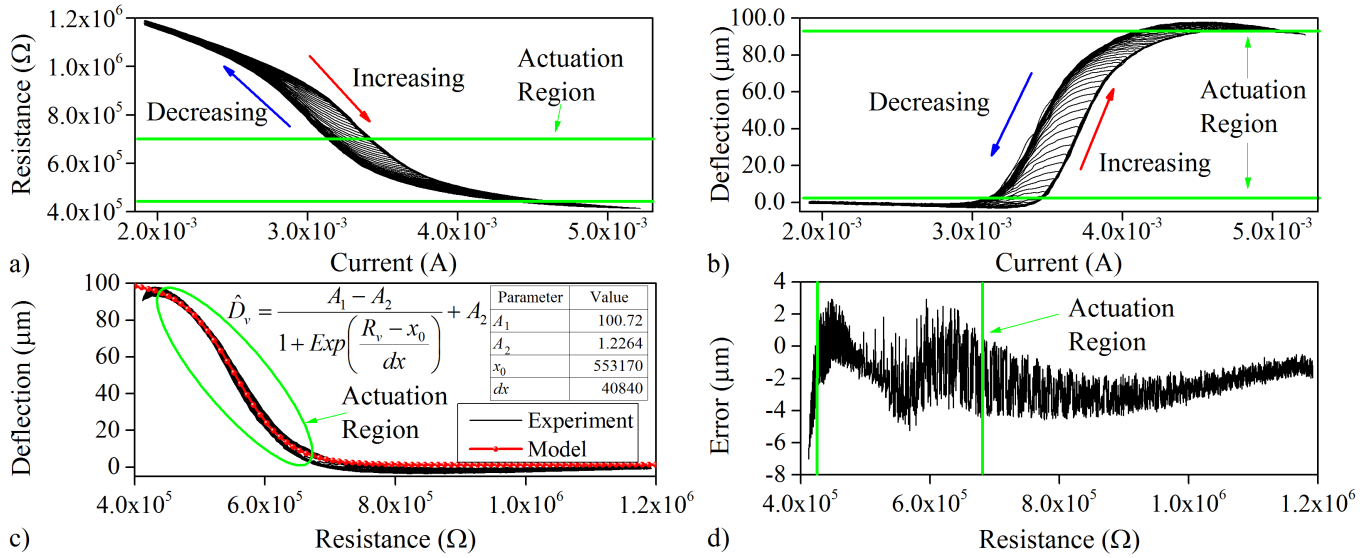

Fig. 3. Quasi-static results for self-sensing model. (a) VO_2 resistance and (b) MEMS actuator deflection as a function of heater current–positive deflection refers to displacement out-of-plane. (c) MEMS actuator deflection as a function of VO_2 resistance and Boltzmann model used with the corresponding parameters. (d) Self-sensing modeling error as a function of VO_2 resistance.

parameters obtained from the fit are shown in an inset table in Figure 3-(c). Figure 3-(d) shows the error between the experimental data and the model in (1). The noise observed in this curve is still to be fully understood. The maximum absolute error produced by the self-sensing model is 5 μm with an average error of −1.1 μm, throughout the complete actuation range of 95 μm. These results show that (1) can accurately estimate D_r and be used as the feedback signal to control the device deflection.

B. System Dynamic Model

In order to design the controller gains that will operate the micro-actuator, an accurate model of the system dynamics is needed. To this end, the setup in Figure 2-b was used to obtain the open-loop magnitude frequency response of the micro-actuator for a sinusoidal input signal. The input frequency was varied from 0.1 to 200 Hz with a constant magnitude and offset of 0.4 mA and 3.6 mA, respectively. These values were chosen in order to include large part of the monotonic increasing deflection across the transition region (see Figure 3-(b)).

Figure 4 shows the deflection and resistance gains (i.e. D_r and R_v gains) of the micro-actuator with respect to the actuation signal, I_h as a function of frequency. The cut-off frequencies for both signals are very close to each other (around 20 Hz), which is expected since the dynamics of the electrical and mechanical parameters in these types of thermally-actuated devices is dominated by thermal dissipation through the anchor and the surrounding media [33]. Furthermore, both signals can be described by a first-order system, since drag and internal mechanic dynamic effects are known to take place at much higher frequencies - more than an order of magnitude higher than the thermal cut-off frequency [33]. The resistance gain is modeled by a first-order transfer function defined here as:

$$G(s) = \frac{A_0}{\tau s + 1}, \tag{2}$$

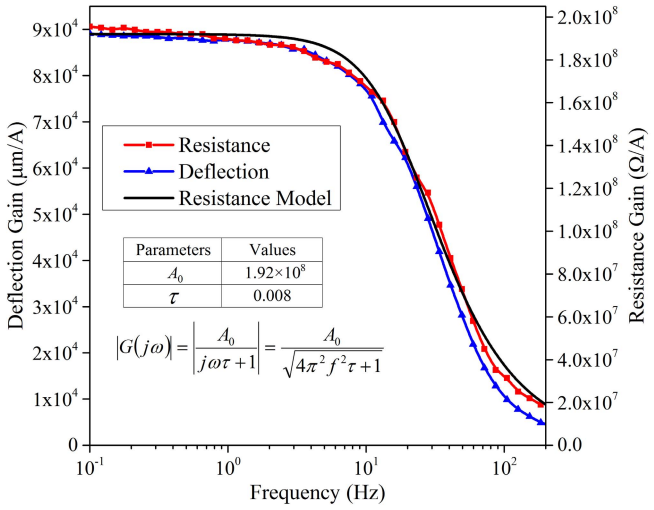

Fig. 4. VO_2 resistance and deflection gains as a function of frequency under open-loop sinusoidal actuation obtained experimentally. The resistance gain is also modeled by a first-order transfer function with parameters shown in the inset table.

where A_0 is the resistance DC gain, and τ is the time constant of the system. In order to find the values for A_0 and τ, the magnitude of (2) is calculated by finding $|G(j\omega)|$ and then fitted with the experimental data. Note that $\omega = 2\pi f$ where f is the linear frequency in units of Hz.

C. PID Controller Design

The self-sensing and dynamic system models were used to determine a set of PI gains that resulted in an accurate and controlled D_r using $\hat{D}_r$. Figure 5-(a) shows the high-level block diagram representation of the micro-actuator system. The controller uses $\hat{D}_r$ (calculated from the self-sensing model using R_v) and the reference deflection value D_{ref} to supply I_h (the control signal) in order to drive the VO_2-MEMS device.

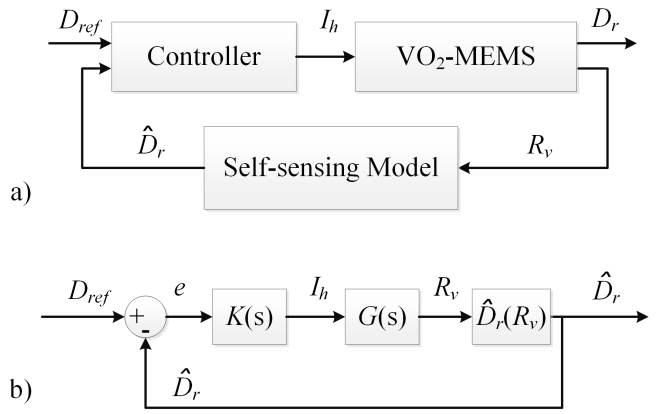

Fig. 5. (a) Simplified high-level and (b) expanded dynamic closed-loop block diagrams of the VO_2-MEMS actuator using self-sensing.

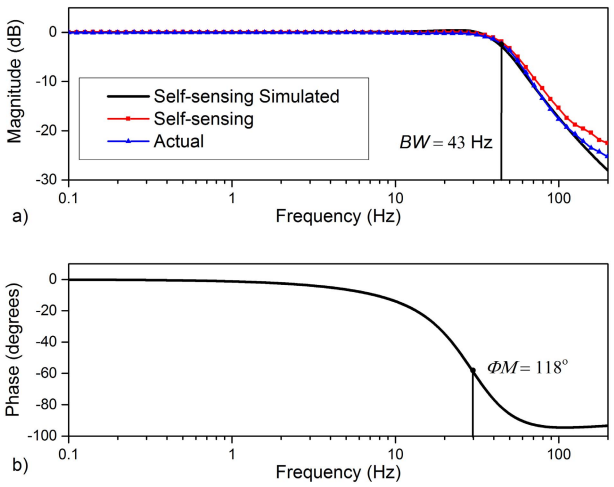

Fig. 6. Experimental and simulated (a) magnitude and (b) phase as a function of frequency of the closed-loop controlled VO_2-based MEMS actuator.

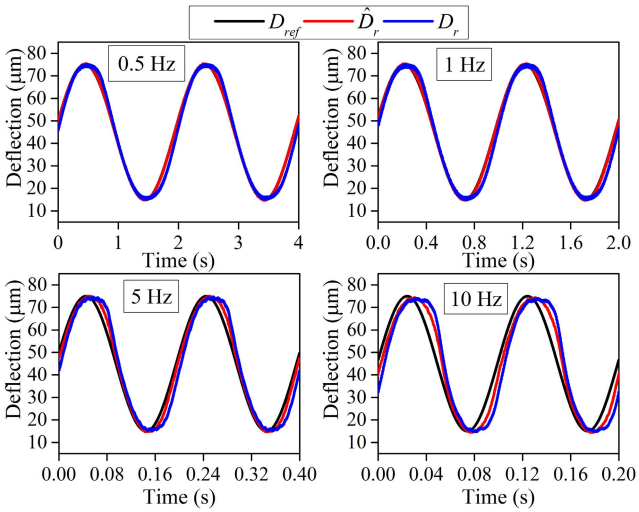

Fig. 7. Sinusoidal time dependent deflection response for the self-sensing and actual values at different frequencies.

Note that D_r is only used to validate the performance of the self-sensing closed-loop system. An expanded view of the self-sensing closed-loop system is shown in Figure 5-(b), where e is the error between D_{ref} and $\hat{D}_r$, $K(s)$ is the PI controller transfer function, $G(s)$ is the resistance transfer function from (2), and $\hat{D}_v(R_v)$ is the self-sensing model from (1). $K(s)$ is defined as

$$K(s) = K_p + \frac{K_i}{s}, \tag{3}$$

where K_p and K_i are the proportional and integral gains, respectively. Since the deflection and resistance open-loop responses have very similar performance in terms of cut-off frequency, a controller designed to compensate $\hat{D}_r$ should also compensate D_r with similar closed-loop performance. Hence, (3) was designed to control the system in Figure 5-(b) in order to achieve a bandwidth (BW) of at least 40 Hz, which is double the open-loop bandwidth, and an overshoot of less than 10 %, which traduces to a phase margin (ΦM) of less than 121°. The obtained gains based on these specifications are $K_p = 0.07$ and $K_i = 87.5$ and the simulated performance of the closed-loop system using these gains is shown in Figure 6-(a-b).

IV. Results and Discussion

To test the performance of the micro-actuator system, a series of reference tracking experiments were performed. First, the closed-loop frequency response was obtained experimentally by applying a sinusoidal reference signal with varying frequency. Second, a step reference input response was used to obtain the transient performance of the system and study the overall system accuracy. Along the discussion of the results, the actual deflection is given more emphasis than the estimated deflection. However, the estimated deflection is also included in the analysis in order to demonstrate the effectiveness of the self-sensing feedback method.

A. Closed-Loop Frequency Response

To experimentally obtain the closed-loop frequency response of the micro-actuator, D_{ref} was chosen as a sinusoidal wave of varying frequency from 0.1 to 200Hz with a magnitude and offset of 30 µm and 45 µm, respectively. Figure 6-(a) shows the magnitude gain in decibels of the closed-loop system for the mentioned input conditions. The self-sensing and actual deflection gains follow the simulated results closely with a BW of 43 Hz.

The effectiveness of the self-sensing model is also verified by the unnoticeable difference between the self-sensing and actual deflection performances before the ΦM (0 dB) frequency of 30 Hz. The maximum difference between D_r and $\hat{D}_r$ is 0.255 dB or 1.8 µm through the deflection range of 60 µm tested in this experiment. In addition, maximum actual and self-sensing errors to that of the setpoint are 0.19 dB (1.32 µm) and 0.015 dB (0.1 µm), respectively.

To further show the frequency and time dependent performance of the micro-actuator, some of the deflection sinusoidal responses used to obtain the results in Figure 6-(a) as a function of time at different frequencies are shown in Figure 7. One noticeable trend is the increased difference between the

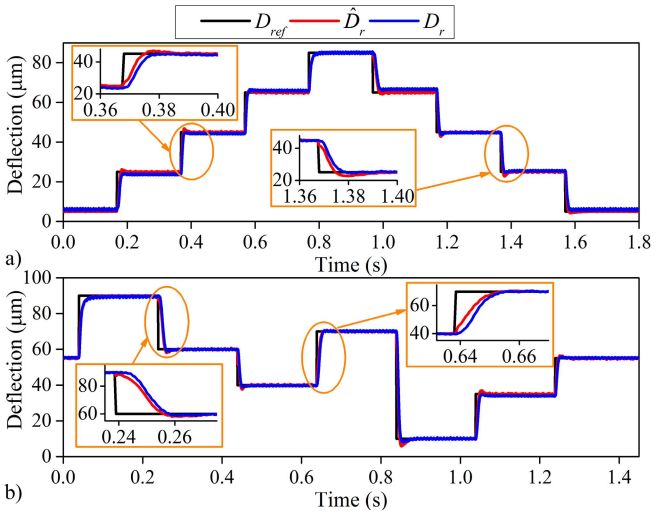

Fig. 8. Step reference input results for the (a) increasing-decreasing loop and (b) arbitrary steps experiments.

actual and setpoint deflection values right after the maximum and minimum setpoint peaks. Hence, it is difficult to obtain a measure of the phase difference, since the phase value varies when calculated at different locations within a period. For example, at 10 Hz the phase difference is 22° if calculated at the sinusoidal offset value or 30° if calculated at the maximum value. One plausible explanation is the asymmetry of the hysteretic curve. The actuation region for this particular frequency response experiment - which is smaller than the actuation region used for the quasi-static experiments shown in Figure 3 - includes a hysteretic region that is non-symmetric. This non-symmetry (which is not modeled by (1)) changes the shape of the limiting cycles in the actuation region; causing pronounced differences between the estimated and actual deflection when cycling between setpoint peaks. This has been observed in a previous sinusoidal control experiment performed by the authors, where the actual deflection was directly controlled [34].

B. Step Reference Tracking

D_{ref} was chosen as two sequences of varying step inputs with duration of 200 ms each in order to study the transient and steady-state errors of the closed-loop controlled VO_2-MEMS actuator. The first sequence was designed to cover one stable hysteresis loop (increasing and then decreasing staircase cycle), while the second sequence was designed to study the performance throughout the hysteresis (arbitrary increasing and decreasing steps). The results for the first and second sequences are shown in Figure 8-(a-b), respectively. Both figures also show inset plots of some step regions in order to show transient behavior.

The effectiveness and accuracy of the self-sensing feedback micro-actuator is evident. An average D_r steady-state error of 1.15 μm is found from all the different steps in both sequences with average system accuracy of ±430 nm. The maximum steady-state error is 1.88 μm from all the setpoint values tested. Rise times — defined here as time taken by D_r to change from 10 to 90% of the step value — ranging from 5 to 12 ms are obtained with maximum percent overshoot of 8.4%. The measured performance of D_r falls within the designed specifications, thus confirming that self-sensing can be used to accurately and effectively control the deflection of VO_2-based MEMS actuators.

V. Conclusion

The strong coupling of the electrical and mechanical properties in VO_2 across its phase transition has been used to allow self-sensing in a VO_2-based MEMS actuator with integrated heater. This technique allowed for the reduction of the hysteresis effects in these devices, simplifying their control. A simple, yet effective, Boltzmann function was used to model the resistance-to-deflection relationship and obtain an estimated deflection value, which was used as feedback to control the actual deflection of the micro-actuator. Sinusoidal and step input tracking experiments were performed in order to show the performance of the micro-actuator in terms of frequency response, transient response and steady-state error.

Further miniaturization can be achieved by utilizing a micro-controller for realizing the closed-loop control, which would result in a fully monolithically integrated system. The performance of the micro-actuator can be enhanced by utilizing more robust controllers, improving the self-sensing model, and optimizing heater location and device fabrication for achieving higher operational bandwidth and accuracy.

Acknowledgment

The fabrication of the microactuator was done at the Lurie Nanofabrication Facility at The Univeristy of Michigan. The SEM images were taken at the Composite Materials and Structures Center at Michigan State University.

References

[1] M. I. Beyaz, M. McCarthy, N. Ghalichechian, and R. Ghodssi, "Closed-loop control of a long-range micropositioner using integrated photodiode sensors," *Sens. Actuators A, Phys.*, vol. 151, no. 2, pp. 187–194, 2009.

[2] M. U. Khan, N. Bencheikh, C. Prelle, F. Lamarque, T. Beutel, and S. Buttgenbach, "A long stroke electromagnetic *XY* positioning stage for micro applications," *IEEE/ASME Trans. Mechatronics*, vol. 17, no. 5, pp. 866–875, Oct. 2012.

[3] Y. Xie, Y. Tan, and R. Dong, "Nonlinear modeling and decoupling control of *XY* micropositioning stages with piezoelectric actuators," *IEEE/ASME Trans. Mechatronics*, vol. 18, no. 3, pp. 821–832, Jun. 2013.

[4] B. Tamadazte, M. Paindavoine, J. Agnus, V. Petrini, and N. Le-Fort Piat, "Four d.o.f. piezoelectric microgripper equipped with a smart CMOS camera," *J. Microelectromech. Syst.*, vol. 21, no. 2, pp. 256–258, Apr. 2012.

[5] T. Chen, L. Chen, L. Sun, and X. Li, "Design and fabrication of a four-arm-structure MEMS gripper," *IEEE Trans. Ind. Electron.*, vol. 56, no. 4, pp. 996–1004, Apr. 2009.

[6] J. Leinvuo, S. Wilson, R. Whatmore, and M. G. Cain, "Flextensional ultrasonic piezoelectric micro-motor," *IEEE Trans. Ultrason., Ferroelectr., Freq. Control*, vol. 53, no. 12, pp. 2357–2366, Dec. 2006.

[7] F. Cros, H. Koser, M. Allen, and J. H. Lang, "Magnetic induction micromachine—Part II: Fabrication and testing," *J. Microelectromech. Syst.*, vol. 15, no. 2, pp. 427–439, 2006.

[8] K. W. Oh and C. H. Ahn, "A review of microvalves," *J. Micromech. Microeng.*, vol. 16, no. 5, pp. R13–R39, 2006.

[9] M. Miled and M. Sawan, "Dielectrophoresis-based integrated lab-on-chip for nano and micro-particles manipulation and capacitive detection," *IEEE Trans. Biomed. Circuits Syst.*, vol. 6, no. 2, pp. 120–132, Apr. 2012.

[10] T. Beutel, N. Ferreira, A. Balck, M. Leester-Schadel, and S. Buttgenbach, "Cell manipulation system based on a self-calibrating silicon micro force sensor providing capillary status monitoring," *IEEE Sensors J.*, vol. 12, no. 10, pp. 3075–3081, Oct. 2012.

[11] S. Schuerle, S. Erni, M. Flink, B. Kratochvil, and B. Nelson, "Three-dimensional magnetic manipulation of micro- and nanostructures for applications in life sciences," *IEEE Trans. Magn.*, vol. 49, no. 1, pp. 321–330, Jan. 2013.

[12] M. Vagia and A. Tzes, "Robust PID control design for an electrostatic micromechanical actuator with structured uncertainty," *IET Control Theory Appl.*, vol. 2, no. 5, pp. 365–373, May 2008.

[13] Y. Shen, E. Winder, N. Xi, C. A. Pomeroy, and U. C. Wejinya, "Closed-loop optimal control-enabled piezoelectric microforce sensors," *IEEE/ASME Trans. Mechatronics*, vol. 11, no. 4, pp. 420–427, Aug. 2006.

[14] G. Song, V. Chaudhry, and C. Batur, "Precision tracking control of shape memory alloy actuators using neural networks and a sliding-mode based robust controller," *Smart Mater. Struct.*, vol. 12, no. 2, pp. 223–231, Feb. 2003.

[15] A. Mannani and H. A. Talebi, "A fuzzy Lyapunov-based control strategy for a macro–micro manipulator: Experimental results," *IEEE Trans. Control Syst. Technol.*, vol. 15, no. 2, pp. 375–383, Mar. 2007.

[16] M. Suster, J. Guo, N. Chaimanonart, W. H. Ko, and D. J. Young, "A high-performance MEMS capacitive strain sensing system," *J. Microelectromech. Syst.*, vol. 15, no. 5, pp. 1069–1077, Oct. 2006.

[17] R. K. Messenger, Q. T. Aten, T. W. McLain, and L. L. Howell, "Piezoresistive feedback control of a MEMS thermal actuator," *J. Microelectromech. Syst.*, vol. 18, no. 6, pp. 1267–1278, Dec. 2009.

[18] C. Hautamaki, L. Cao, J. Zhou, S. C. Mantell, and T. S. Kim, "Calibration of MEMS strain sensors fabricated on silicon: Theory and experiments," *J. Microelectromech. Syst.*, vol. 12, no. 5, pp. 720–727, Oct. 2003.

[19] A. Rua, F. E. Fernandez, and N. Sepulveda, "Bending in VO_2-coated microcantilevers suitable for thermally activated actuators," *J. Appl. Phys.*, vol. 107, no. 7, pp. 074506-1–074506-4, Apr. 2010.

[20] F. Amiot and J. P. Roger, "Nomarski imaging interferometry to measure the displacement field of micro-electro-mechanical systems," *Appl. Opt.*, vol. 45, no. 30, pp. 7800–7810, 2006.

[21] J. Ouyang and Y. Zhu, "Z-shaped MEMS thermal actuators: Piezoresistive self-sensing and preliminary results for feedback control," *J. Microelectromech. Syst.*, vol. 21, no. 3, pp. 596–604, 2012.

[22] C. C. Lan and C. H. Fan, "An accurate self-sensing method for the control of shape memory alloy actuated flexures," *Sens. Actuators A, Phys.*, vol. 163, no. 1, pp. 323–332, 2010.

[23] A. Kawamata, Y. Kadota, H. Hosaka, and T. Morita, "Self-sensing piezoelectric actuator using permittivity detection," *Ferroelectrics*, vol. 368, no. 1, pp. 194–201, 2008.

[24] I. A. Ivan, M. Rakotondrabe, P. Lutz, and N. Chaillet, "Current integration force and displacement self-sensing method for cantilevered piezoelectric actuators," *Rev. Sci. Instrum.*, vol. 80, no. 12, pp. 126103-1–126103-3, 2009.

[25] B. K. Nguyen and K. K. Ahn, "Feedforward control of shape memory alloy actuators using fuzzy-based inverse Preisach model," *IEEE Trans. Control Syst. Technol.*, vol. 17, no. 2, pp. 434–441, Mar. 2009.

[26] T. M. Wang, Z. Y. Shi, D. Liu, C. Ma, and Z. H. Zhang, "An accurately controlled antagonistic shape memory alloy actuator with self-sensing," *Sensors*, vol. 12, no. 6, pp. 7682–7700, 2012.

[27] H. Ikeda and T. Morita, "High-precision positioning using a self-sensing piezoelectric actuator control with a differential detection method," *Sens. Actuators A, Phys.*, vol. 170, nos. 1–2, pp. 147–155, 2011.

[28] E. Merced, J. Zhang, X. Tan, and N. Sepulveda, "Robust control of VO_2-coated microbenders using self-sensing feedback," *IEEE/ASME Trans. Mechatronics*, to be published, doi: 10.1109/TMECH.2013.2289375.

[29] F. J. Morin, "Oxides which show a metal-to-insulator transition at the neel temperature," *Phys. Rev. Lett.*, vol. 3, no. 1, pp. 34–36, 1959.

[30] J. Barker, Jr., H. W. Verleur, and H. J. Guggenheim, "Infrared optical properties of vanadium dioxide above and below the transition temperature," *Phys. Rev. Lett.*, vol. 17, no. 26, pp. 1286–1289, 1966.

[31] E. Merced, X. Tan, and N. Sepúlveda, "Strain energy density of VO_2-based microactuators," *Sens. Actuators A, Phys.*, vol. 196, pp. 30–37, Jul. 2013.

[32] R. Cabrera, E. Merced, and N. Sepúlveda, "A micro-electro-mechanical memory based on the structural phase transition of VO_2," *Phys. Status Solidi A*, vol. 210, no. 9, pp. 1704–1711, 2013.

[33] R. Cabrera, E. Merced, and N. Sepúlveda, "Performance of electrothermally driven VO_2-based MEMS actuators," *J. Microelectromech. Syst.*, vol. 23, no. 1, pp. 243–251, 2013.

[34] E. Merced, X. Tan, and N. Sepúlveda, "Closed-loop tracking of large displacements in electrothermally actuated VO_2-based mems," *J. Microelectromech. Syst.*, to be published, doi: 10.1109/JMEMS.2014.2304694.

Emmanuelle Merced (S'13) received the B.Sc. and M.Sc. degrees in electrical engineering from the University of Puerto Rico, Mayagüez, Puerto Rico, in 2009 and 2011, respectively. He is currently working towards the Ph.D. degree in the Department of Electrical and Computer Engineering, Michigan State University, East Lansing, MI, USA. He has participated in numerous research and industry related programs including: Memristor group intern at Hewlett-Packard Laboratories, Palo Alto, CA (2013), independent contractor at Universal Technology Corporation, Dayton, OH (2011), research intern at the United States Army Corps of Engineers, Vicksburg, MS (2009), and research intern at the Power System and Automation Laboratory at Texas A&M University, College Station, TX (2008), among others. His research interests include design, fabrication, and implementation of microelectromechanical (MEMS) actuators, smart materials-based microtransducers, control systems of hysteretic systems, and tunable microresonators.

Dr. Merced was awarded the National Science Foundation Graduate Research Fellowship in 2011 and was named the Electrical Engineering Outstanding Graduate Student for 2012-2013.

David Torres received his B.S. degree in Electrical and Computer Engineering from the University of Puerto Rico, Mayaguez, Puerto Rico, in December 2012. He is currently working towards his Ph.D. degree in the Department of Electrical and Computer Engineering, Michigan State University, East Lansing, MI, USA. He participated in a number of research projects as an undergraduate student including a summer research internship at MSU. His current research interests include design, fabrication, and implementation of micro-electro-mechanical actuators and control of hysteretic systems.

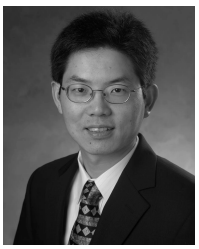

Xiaobo Tan (S'97–M'02–SM'11) received the B.Eng. and M.Eng. degrees in automatic control from Tsinghua University, Beijing, China, in 1995 and 1998, respectively, and the Ph.D. degree in electrical and computer engineering from the University of Maryland, College Park, MD, USA, in 2002.

From September 2002 to July 2004, he was a Research Associate with the Institute for Systems Research, University of Maryland. He joined the faculty of the Department of Electrical and Computer Engineering, Michigan State University (MSU), East Lansing, MI, USA, in 2004, where he is currently an Associate Professor. His research interests include electroactive polymer sensors and actuators, modeling and control of smart materials, biomimetic robotic fish, mobile sensing in aquatic environments, and collaborative control of autonomous systems.

Dr. Tan is an Associate Editor of *Automatica*, Associate Editor of *International Journal of Advanced Robotic Systems*, and Technical Editor of IEEE/ASME TRANSACTION ON MECHATRONICS. He served as the Program Chair for the 15th International Conference on Advanced Robotics in 2011, and is serving as the Finance Chair for 2015 American Control Conference. He served as a guest editor for IEEE CONTROL SYSTEMS MAGAZINE and the *Journal of Robotics and Autonomous Systems*. He received a National Science Foundation CAREER Award in 2006, the Teacher-Scholar Award from MSU in 2010, and several best paper awards during 2009-2013.

Nelson Sepúlveda (S'05–M'06–SM'11) received the B.S. degree in electrical and computer engineering from the University of Puerto Rico, Mayagüez, Puerto Rico, in 2001, and the M.S. and Ph.D. degrees in electrical and computer engineering from Michigan State University (MSU), East Lansing, MI, USA, in 2002 and 2005, respectively. During the last year of graduate school, he attended the Sandia National Laboratories as part of a fellowship from the Microsystems and Engineering Sciences Applications program.

In January 2006, he joined the faculty of the Department of Electrical and Computer Engineering, University of Puerto Rico. He has been a Visiting Faculty Researcher at the Air Force Research Laboratories (2006, 2007, 2013, and 2014), National Nanotechnology Infrastructure Network (2008), and the Cornell Center for Materials Research (2009), the last two being the National Science Foundation (NSF) funded centers at Cornell University, Ithaca, NY, USA. In Fall 2011, he joined the faculty of the Department of Electrical and Computer Engineering, MSU, where he is currently an Assistant Professor. His current research interests include smart materials and the integration of such in microelectromechanical systems, with particular emphasis on vanadium dioxide (VO_2) thin films and the use of the structural phase transition for the development of smart microactuators.

Dr. Sepúlveda received an NSF CAREER Award in 2010.